Progesterone limits the tumor-promoting effects of the beta-subunit of human chorionic gonadotropin via non-nuclear receptors

Moumita Sarkar
National Institute of Immunology
Harsh Sharma
Amity University
Parminder Singh
Buck Institute for Age Research: Buck Institute for Research on Aging
Ranbala Ranu
National Institute of Pathology
Ravi Datta Sharma
Amity University
Usha Agrawal
National Institute of Pathology
Rahul Pal (rahul@nii.ac.in)
National Institute of Immunology

Research Article

Keywords: Post-menopausal women, tumorigenesis, beta-hCG, progesterone, non-nuclear receptors, apoptosis, transcriptome profiling, TCGA analysis

Posted Date: February 22nd, 2022

DOI: https://doi.org/10.21203/rs.3.rs-1368962/v1

Abstract

Background Beta-hCG can be detected in post-menopausal women, who also demonstrate an increased cancer risk. Whether ovarian hormones mediate cytotoxic effects on beta-hCG-responsive tumor cells, whether beta-hCG exerts enhanced pro-tumorigenic effects in the absence of ovarian steroids, and whether steroid administration can have restorative effects on tumor molecular profiles and progression, remain unaddressed.

Methods The effect of ovarian steroids on the proliferation, viability and apoptosis of beta-hCG responsive LLC1 tumor cells were assessed. Involvement of nuclear/non-nuclear steroid receptors was evaluated by assessing presence and employing receptor antagonists, by cAMP measurements, and by assessing MAP kinase activation. LLC1 tumor cells were implanted in female non-transgenic mice, in beta-hCG transgenic mice and in ovariectomized beta-hCG transgenic mice; progesterone was additionally administered to the latter two groups. Tumor volumes were measured, and RNA-seq, qPCR and immunohistochemistry were employed to characterize tumor molecular profiles. TCGA databases for lung adenocarcinoma, colon adenocarcinoma and glioblastoma were probed with human orthologs of newly-identified genes to reveal clinically-relevant associations, with a focus on the post-menopausal state.

Results Ovarian steroids demonstrated anti-tumor effects in vitro; progesterone caused tumor cell apoptosis via non-nuclear receptors and the phosphorylation of p38. Beta-hCG, particularly in absence of the ovaries (a mimic of the post-menopausal state), constituted an aggravated pro-tumorigenic signal for implanted LLC1 tumor cells. Progesterone dampened aggravated tumor growth in ovariectomized mice. RNA-seq on excised tumors identified genes associated with enhanced beta-hCG-mediated tumor growth in ovariectomized mice, as well as with the anti-tumor effects of progesterone. TCGA analysis revealed correlations between the expression of several newly-identified, progesterone-influenced genes (and of intra-tumoral beta-hCG) and poor patient prognosis, specifically in post-menopausal women.

Conclusion This study describes a previously-unidentified interplay between progesterone and beta-hCG in the regulation of tumorigenesis. Murine tumor-associated gene signatures, combined with queries on aggressive human tumors reveal, for the first time, that beta-hCG acts as an additionally potent pro-tumorigenic signal when the ovaries are quiescent. Associations of progesterone-influenced genes (and intra-tumoral beta-hCG) with prognosis were revealed. Intra-tumoral / extra-tumoral beta-hCG may be a useful prognostic indicator in post-menopausal women with cancer, and progesterone may constitute a potential therapeutic in such cases.

Background

During menopause, the ovaries lose the ability to respond to pituitary hormones, resulting in a cessation in the production of ovarian steroids. The post-menopausal state can be accompanied by several clinical symptoms [1]. In particular, post-menopausal women display a higher risk of cancers of different

lineages, such as of the lung and colon [2, 3]. The risk of glioma and breast carcinoma is also enhanced, being also influenced by age at menarche and menopause [4, 5]. The number of deaths due to cancer in postmenopausal women is expected to increase by 70% in the next 20 years, and the understanding of post-menopausal biology as it relates to clinical management of cancer is therefore of some importance.

Interestingly post-menopausal women frequently display elevated levels of either hormone human chorionic gonadotropin (hCG) [6, 7] or its beta subunit (beta-hCG) [8, 9], believed to be of pituitary origin [7–9]. The presence of beta-hCG could be indicative of ectopic implantation [10], the presence of germ cell or gestational tumors [11, 12], or of certain non-trophoblastic neoplasias [13]. While placental hCG has well-established physiological roles in pregnancy, the hormone (or more commonly beta-hCG) is also ectopically produced by tumors and may possess pro-tumorigenic attributes [13–16]. For example, hCG or its beta subunit can positively influence neoplastic transformation by aiding processes such as invasion, metastasis and chemoresistance [17–21]. Of note, the presence of beta-hCG in cancer patients has been associated with tumor aggressiveness [22, 23] and with poor prognosis [20, 24].

The correlation between the presence of beta-hCG, the post-menopausal state and the risk of oncogenesis remains enigmatic, and whether ovarian steroids can mediate a protective role is worthy of investigation. This work attempted to shed some light on this matter. *In vitro* studies demonstrated the apoptosis-inducing effects of ovarian steroids on beta-hCG responsive tumor cells; a subsequent focus on progesterone led to delineation of the mechanisms of cytotoxic action mediated by the steroid. Two observations were of significance; firstly, the cytotoxic effects of progesterone were mediated via non-nuclear receptors, and secondly, neither hCG not beta-hCG could inhibit the cytotoxic effects of progesterone on tumor cells, unlike their protective effects against a conventional chemotherapeutic drug.

Beta-hCG transgenic mice provided an ideal model for the critical evaluation of the anti-tumor effects of progesterone *in vivo*; ovariectomy in such mice could serve as a mimic of the post-menopausal state, where implanted tumors would be exposed to beta-hCG in the absence of ovarian steroids. The fact that tumors cells grew more aggressively in ovariectomized animals was instructive. Further, the administration of progesterone to ovariectomized, tumor cell-implanted beta-hCG transgenic mice effectively reversed the exaggerated tumor growth induced upon ovariectomy. Essentially, progesterone appeared to compensate for the lack of the ovaries.

Transcriptome profiling of tumors isolated from transgenic mice, ovariectomized transgenic mice, as well as from ovariectomized transgenic mice treated with progesterone, added another dimension to this study. The identity of several well-known pro-tumorigenic and anti-tumorigenic genes that were modulated both as a consequence of ovariectomy, as well as by the action of progesterone (in a beta-hCG-containing milieu) was revealed. Additionally, reference to TCGA databases provided critical clinical relevance in the context of some aggressive human cancers, particularly relevant to post-menopausal status; the expression of beta-hCG, as well as of several progesterone-influenced tumor-associated genes identified in the ovariectomized transgenic murine model, correlated with poorer prognosis specifically in post-menopausal women, as compared to the pre-menopausal cohort.

These findings are novel, and of potential clinical significance. This study associates a previously unidentified negative attribute to beta-hCG post-menopause. Collectively, they suggest that, in post-menopausal women, the combination of low progesterone and an increase in beta-hCG can enhance cancer progression. Progesterone mediates significant anti-tumor effects in a beta-hCG containing milieu in mice, acting via non-nuclear receptors; analysis of TCGA databases revealed that tumors in post-menopausal women also express such receptors. The data reported here strengthens the case for progesterone-based therapeutics in beta-hCG expressing post-menopausal women with cancer.

Methods

Cell lines

LL/2 (LLC1) (ATCC) and A549 (ATCC) tumor cells were maintained in DMEM, high glucose (Gibco) supplemented with 3.7g/l sodium bicarbonate, 1% antibiotic-antimycotic (Gibco), and 10% FBS (heat-inactivated). For subculture, trypsin-EDTA (Gibco) was used and cells were regularly checked for mycoplasma contamination. To lower endogenous hormone action in cells prior to steroid treatment, cultures were maintained for an additional 24 h in the medium containing charcoal-stripped fetal bovine serum (FBS, Himedia) instead of regular FBS. Henceforth, this particular media formulation has been referred to as serum-reduced media and all treatments in this study were added in this media. Cells were used within six months of purchase and resuscitation.

Mice

Eight-week old C57BL/6 female mice (procured from The Jackson Laboratory, USA) were outbred with eight-week old FVB male beta-hCG heterozygous transgenic mice, the latter a kind gift from Dr. Ilpo Huhtaniemi, Imperial College, UK; the transgenic mice express the beta-hCG transgene under the ubiquitin promoter. F1 female pups were weaned at 21 days and screened by genomic PCR for detection of the beta-hCG transgene and by radioimmunoassay for estimation of serum beta-hCG levels.

Cell viability

MTT

8×10^3 LLC1 tumor cells (12×10^3 for A549) were seeded onto 96 well plates for 6 h and after completion of respective treatments, the spent media was carefully removed from each well. 50 ml of 0.5 mg/ml MTT (Invitrogen) was added to cells for 1 h followed by 3 h incubation at 37°C with 100 ml DMSO (Amresco). The absorbance was recorded at 570 nm using Gen5 BioTek spectrometer. Reading of “blank” wells were subtracted from all values and percentage viability in comparison with relevant controls was calculated.

ATP measurement

16×10^3 LLC1 tumor cells were cultured in 24 well-plates for 8 h. Post completion of desired treatments, CellTiter-Glo® 2.0 Cell Viability Assay (Promega) was performed following the manufacturer's protocol with slight optimizations. Briefly, the plate and the commercial reagent to be added was equilibrated at 22°C for 15 min. The spent media was removed and the cells were washed with PBS. The pre-equilibrated reagent (provided in the kit) was reconstituted in serum-free DMEM in the ratio 1:1; this solution was added to each well followed, by an incubation for 2 min on a plate shaker. The plate was incubated at 22°C for an additional 10 min. The constituents of each well were collected and centrifuged at 400 g for 5 min at 4°C. The upper fraction was transferred into Thermo Scientific™ Nunc™ F96 MicroWell™ white polystyrene plate. The luminescence (indicative of cell viability) was measured using Synergy H1 multimode plate reader. Percentage viability in comparison with relevant controls was calculated.

Cell proliferation

15×10^3 LLC1 tumor cells (20×10^3 for A549) cultured in 96-well plates for 6 h. 18 h before completion of respective treatment, 0.5 mCi / 50 ml ^{3}H-Thymidine (American Radiolabeled Chemicals) was added onto each well. Cell-associated radioactivity was assessed using a beta-counter (Perkin Elmer).

Apoptosis

Flow cytometry

LLC1 tumor cells, cultured in 96-well plates, were treated with 100 ml accutase (Gibco) for 6 min to allow gentle detachment of cells. 150 ml of serum-free DMEM was then added to each well. The constituents of each well were collected and centrifuged at 100 g for 5 min at 4 °C. The pellet was washed twice with cold PBS and reconstituted in 100 ml Annexin-V binding buffer (BD Biosciences). The constituents were transferred to FACS tubes and 5 ml PE-conjugated Annexin-V (BD Biosciences) was added to the samples. The tubes were subjected to gentle pulse vortexing to attain a single-cell suspension. The tubes were incubated in the dark for 15 min at room temperature. The samples were reconstituted in 500 ml Annexin-V binding buffer and incubated for an additional 15 min. Samples were then analyzed by flow cytometry, after appropriate gating to avoid debris. FlowJo software was used for data analysis and the percentage of Annexin-V positive cells calculated.

Immunofluorescence microscopy

To enhance attachment of LLC1 tumor cells, coverslips were immersed in 1M HCl for 8 h, washed with water, immersed in 70% ethanol and then exposed to UV light for 20 min. Coverslips were placed in 24-well plates. 20×10^3 LLC1 tumor cells were then seeded, and cultured for 8 h. After completion of respective treatments, cells were washed with cold PBS. 200 ml Annexin-V binding buffer containing 7 ml FITC-conjugated Annexin-V (BD Biosciences) and 4 ml propidium iodide (100 mg/ml) (Invitrogen) were added to the wells. An incubation was carried out for 15 min followed by washes with cold Annexin-V binding buffer. DPX (Sigma-Aldrich) was used for mounting. An AxioImager Z1 microscope Carl Zeiss was used for capturing images.

RNA extraction, semi-quantitative PCR and qPCR

Cells and tissues were lysed using TRIzol (Thermo Fisher Scientific) and to attain complete dissociation of nucleoprotein complexes, the samples were allowed to stand for 5 min at room-temperature. 300 ml chloroform (Sigma-Aldrich) per ml TRIzol was added to the tubes. Samples were vigorously shaken and allowed to stand for 20 min at room temperature. The tubes were then centrifuged at 12,000 g for 15 min at 4°C and the upper aqueous phase was transferred to a fresh tube. 500 ml of 2-propanol (Sigma-Aldrich) per ml of TRIzol was added to the samples and the contents were gently mixed and allowed to stand for 15 min at room temperature. The tubes were centrifuged at 12,000 g for 10 min at 4°C. The pellet was washed with 75% pre-chilled ethanol and dried at 60°C in a dry bath for 10 min. The ethanol-free pellet was dissolved in nuclease-free water (Promega). To assure complete dissolution of RNA, the tubes were placed in a dry bath maintained at 65°C for 5 min. The RNA was quantified spectrophotometrically. cDNA was obtained using Verso cDNA synthesis kit (Thermo Fisher Scientific). PRIMER-BLAST was employed for primer designing and the quality of the primers were checked using OligoAnalyzer^{TM} Tool. Semi-quantitative PCR and qPCR were performed by using the primers listed in Supplementary Table S1. The enzyme 3B DNA Polymerase (Biotools) and FG-power SYBR Green PCR master mix (Thermo Fisher Scientific) were used for semi-quantitative PCR and qPCR respectively. The ΔΔCt method was applied for quantification of relative mRNA levels.

cAMP assay

The kit manufacturer's {cAMP glo assay kit (Promega)} instructions were followed, with some modifications. Briefly, 16×10^3 LLC1 tumor cells were seeded onto 24-well plates for 8 h and were cultured for an additional 24 h in serum-reduced media. Cells were then incubated with serum-free media containing 500 mM IBMX (Calbiochem) and 100 mM Ro-20-1724 (Calbiochem) for 30 min to inhibit cellular phosphodiesterase. Test moieties were added in serum-free media; after completion of treatment, spent medium was removed and the cells were washed with PBS. 150 ml of induction buffer (containing similar concentrations of IBMX and RO prepared in PBS) and 150 ml of lysis buffer (provided in the kit) was added to cells. To ensure complete lysis of cells, the plates were placed on a plate shaker for 20 min

at room temperature. The constituents of each well were collected separately in tubes and centrifuged at 400 g for 5 min at 4°C. 40 ml of each supernatant was transferred into Thermo Scientific™ Nunc™ F96 MicroWell™ white polystyrene plate. The remaining steps were conducted as per the manufacture's protocol. Luminescence was measured using Synergy H1 multimode plate reader. The concentration of cAMP was calculated using "Quest Graph™ Four Parameter Logistic (4PL) Curve Calculator.

Western blot

50 to 70 × 10^3 LLC1 tumor cells were seeded onto 6-well plates for 8 h, followed by an additional culture for 24 h in serum-reduced media. After completion of the respective treatments with test moieties, cells were lysed using 600 ml RIPA buffer (150 mM Sodium Chloride, 1% Triton X-100, 0.5% Sodium Deoxycholate, 0.1% SDS, 50 mM Tris Cl, pH 7.4) containing protease inhibitors (Thermo Fisher Scientific). For MAPK detection, phosphatase inhibitors (Thermo Fisher Scientific) were also employed along with the protease inhibitors. To obtain efficient lysis, samples were incubated on ice for 20 min with occasional vortexing and were then sonicated at 4°C using Bioruptor Plus (Diagenode). Lysates were then centrifuged at 10,000 g for 20 min at 4°C. Supernatants were collected and the total protein was estimated using BCA kit (Thermo Fisher Scientific). 35 mg (for MAPKs detection) and 40 mg (for caspase detection) of protein was loaded onto gels and subjected to SDS-PAGE, followed by transfer to nitrocellulose membranes (Biorad). The blots were "blocked" at room temperature for 3 h with 5% skimmed milk (BD Biosciences) in TBS (for caspase detection) and 5% BSA (Merck) in TBS (for MAPKs detection) followed by a 16 to 18 h incubation at 4°C with primary antibodies reconstituted in 5% skimmed milk in 0.1% TBST (for caspase detection) and 5% BSA in 0.1% TBST (for MAPKs detection). The blots were incubated for 1 h with HRP-labelled secondary antibodies at room temperature. ECL (Biorad) exposure was carried out for 5 min and the chemiluminescent signals on the blots were captured using X-ray film (Carestream). Band intensities were calculated using ImageJ.

Genomic DNA isolation and PCR

Murine genomic DNA was isolated by the salted-out method. Briefly, tail clips of mice were collected and incubated in 300 ml digestion buffer (10 mM Tris-Cl; pH 7.5, 400 mM NaCl, 100 mM EDTA, 0.6% SDS) containing 25 ml proteinase K (Qiagen) at 55°C in a dry bath for 8 h. 100 ml of 5.1 M NaCl was added and contents were mixed by inverting the tubes till the solution appeared milky. The samples were centrifuged at 12,000 g for 6 min and supernatant was transferred to a fresh tube. To the clear supernatant, double volume of chilled 95% ethanol (Merck) was added and the contents were mixed gently. The samples were further incubated for 30 min at -20°C followed by centrifugation at 4°C for 20 min at 12, 800 g. The pellet was washed thrice with 70% ethanol. Excess ethanol was evaporated by heating samples at 65°C for 10 min. The DNA was reconstituted in nuclease-free water and the samples were placed at 65°C for an additional 15 min to ensure complete dissolution of DNA. The quality of DNA

was assessed spectrophotometrically. PCR for beta-hCG was carried out using 150 ng of DNA; primers are listed in Supplementary Table S1. The enzyme 3B DNA Polymerase was employed, and 2% DMSO (Sigma-Aldrich) was added to the PCR master mix, owing to the primer's high GC content.

Radioimmunoassay (RIA)

A Sephadex G-75 column (0.9 × 12 cm) was equilibrated with RIA buffer (0.125% $NaH_2PO_4.H_20$, 0.6% Na_2HPO_4, 0.88% NaCl, 0.1 % NaN_3, and 0.1% BSA; pH 7.4). Purified hCG (10,000 IU/mg) was labelled with $Na^{125}I$ by the Iodogen method. Briefly, 25 ml of 0.5 M PBS, hCG (5 mg/10 ml) and 500 mCi $Na^{125}I$ (Perkin Elmer) were added to a glass tube into which 5 mg Iodogen (Thermo Fisher Scientific) had been previously adsorbed. After 10 min, the reaction mixture along with 10 ml of 2% KI (Sigma-Aldrich) was transferred onto the G-75 column to separate iodinated hormone from free radioiodine. 0.5 ml fractions were collected and radioactivity was assessed using gamma counter (Perkin Elmer). The first peak comprised radioactive iodinated hCG (^{125}I-hCG) and the second peak of free iodine.

RIA was performed to quantify beta-hCG in sera derived from transgenic and non-transgenic mice. A murine monoclonal antibody (designated PIPP) was employed for this purpose. Sera, diluted in RIA buffer (1:10) were incubated with an optimum concentration of PIPP, 100 ml of 20% normal horse serum and ^{125}I-hCG (40 µCi/µg, 10,000 CPM) at 4°C for 16 h. 500 ml of 25% polyethylene glycol (Mw 8000; Sigma-Aldrich) was added to all tubes and centrifuged at 600 g at 6°C for 20 min to precipitate immune-complexes. Supernatants were decanted and radioactivity in the pellet was assessed on a gamma counter (Perkin Elmer). Pure hCG (1.25-40 ng/ml) was employed as a standard and serum beta-hCG was quantified by comparisons with the standard curve obtained upon linear regression.

Ovariectomy

Mice selected for this surgical procedure were 5-6 months old. Briefly, animals were anesthetized by intraperitoneal injection of Ketamine (Troikaa Pharmaceuticals Ltd.) and Xylazine (Indian Immunologicals Ltd.) in the ratio 4:1. The constituents of the anesthetic formulation were diluted with an equal volume of autoclaved water. The volume of the injection (ml) was determined based on body-weight (g); three times the body-weight was found optimum. To maintain optimum body-temperature during surgery, the animal was rested on a heating pad. The footpad of the animal was gently pressed to ensure desensitization. On the dorsal side, the animal was shaved and the skin was disinfected with 70% ethanol. A single small incision was made and the musculatures were separated using curved tip scissors. Each ovarian fat pad was carefully pulled out of the incision and the ovaries removed. To ensure real-time blood vessel ligation and minimum blood loss due to surgery, electrocauterization (using

cautery system, Gemini) was employed. The surgical cut was closed using 9 mm surgical clips (Stoelting) and povidone-iodine solution 10% w/v (Betadine) was topically applied. Until recovery from anesthesia, the animals were placed on the heating pad. An ibuprofen and paracetamol suspension (CIPLA; (1 ml/100 ml) was added to the drinking water for 2 days. To hasten recovery, animals were given a daily gavage of 0.9% NaCl. After 10 days of surgery, surgical clips were removed using a clip remover (Stoelting). The efficacy of the surgery was confirmed by checking serum prolactin levels by ELISA (R&D Systems).

Tumor cell implantation

The dorsal side of the animal was shaved a day ahead of implantation and the area was inspected to ensure there was no evidence of skin allergy or local inflammation. 40,000 LLC1 tumor cells (suspended in serum-free DMEM) was subcutaneously injected using a 26G needle. Tumors were measured using a digital caliper. The volumes of the subcutaneously xenografted tumors were calculated by use of the modified ellipsoid formula 1/2(Length × Width^2); w: smaller value of the two-perpendicular tumor axes. At 30 days post-implantation, mice were euthanized and excised pieces of each tumor were collected separately in RNAlater (Qiagen) for RNA-based studies, and in 10% formalin for histochemical analysis.

Progesterone supplementation

Intra-peritoneal supplementation of progesterone or vehicle was initiated on the same day as LLC1 tumor cell implantation in the designated subsets of mice. Briefly, progesterone (Sigma-Aldrich; 100 mg/kg body weight) was reconstituted in 0.1% ethanol in saline (0.9% NaCl) and administered daily using a 26G needle and a glass syringe; treatment was carried out over 21 days.

RNA-seq and Differential Gene Expression Analysis

RNA-seq library preparation was performed at Genotypic Technology’s genomics facility as per NEBNext Ultra directional RNA Library Prep kit. Briefly, RNA was isolated by the TRIzol standard extraction protocol. RNA concentration and purity of samples were estimated using Nanodrop Spectrophotometer and Qubit Fluromter. RNA integrity (RIN) of the samples were analysed using Agilent Bioanalyser. Only samples having RIN > 7 were considered for sequencing. Sequencing was performed using the platform Illumina HiSeq Paired-end sequencing with 150*2. From a total of 188,378,143 Illumina reads, 181,889,366 million high quality reads were used in downstream analysis. Average of 97.21% of the reads were aligned to the reference genome. The raw data generated was checked for the quality using FastQC. Reads were pre-processed to remove the adapter sequences and removal of the low-quality bases (<q30). Pre-processing of the data was done with Trimgalore. HISAT2 which is a splice aligner was used to align the high-quality data to the reference genome with the default parameters. Reads were classified into aligned reads

(which align to the reference genome) and unaligned reads. HTSeq was used to estimate and calculate gene abundance. Absolute counts for each gene were identified which were used in differential expression calculations. DESeq was used to calculate the differentially expressed genes. Genes were categorized into Up, Down and Neutrally regulated based on the log2fold change cut-off value of 1. From this total gene set, only significantly differentially expressed genes with adjusted P-value of ≤ 0.4 and gene expression value of ≥ 30 were finally selected. Jvenn was employed for Venn diagram analysis to identify putative progesterone-influenced genes in tumors. DAVID database and literature review enabled functional annotation of the genes as “pro-tumorigenic” and “anti-tumorigenic”.

Immunohistochemistry

3 µm sections were cut from paraffin-embedded tumors. Slides were placed in an incubator for 1 h at 55°C and then deparaffinized using xylene. To rehydrate the samples, the slides were sequentially exposed to ethanol (90% / 70% / 50%) lastly to water. For antigen retrieval, the slides were placed in Tris-EDTA buffer for 20 min inside a water bath maintained at 95°C. The slides were then washed with TBS and placed in 3% H_2O_2 for 10 min. After washing with TBST, the samples were incubated with primary antibodies at 4°C in a moist chamber for 8 h. After further washes, HRP-labelled secondary antibodies was added. After 2 h, the sections were washed and DAB (freshly-prepared) was added for 10 min. Sections were then washed with water. Slides were then counter-stained with hemotoxylin and mounted using DPX. All reagents used in this assay was contained in the kit (DAKO, K8002). Images were captured using ZEISS Axio Imager Z2.

TCGA analysis

STAR-aligned RNA-Sequencing reads for colorectal cancer (TCGA-COAD, n=521) (https://doi.org/10.1038/nature11252), and glioblastoma (TCGA-GBM, n=174) (https://doi.org/10.1038/nature07385) were downloaded as bam files from the TCGA GDC data portal (https://portal.gdc.cancer.gov). Differential gene expressions of these datasets was analyzed using the FASE pipeline (https://github.com/harshsharma-cb/FASE), and log2CPM expression was obtained. For lung cancer (TCGA-LUAD, n=576) (https://doi.org/10.1038/nature13385), TPM expression was downloaded from (https://gdac.broadinstitute.org). Clinical data for the cancers was downloaded from the GDC data portal (https://gdac.broadinstitute.org). For the downstream analyses, R statistical software {R Core Team (2019). R: A language and environment for statistical computing. R Foundation for Statistical Computing, Vienna, Austria. URL https://www.R-project.org/} was employed. For survival analysis, the survival package of R {Therneau T (2015). _A Package for Survival Analysis in S_. version 2.38, <URL: https://CRAN.R-project.org/package=survival>} was employed. To find optimum cut-off value for dividing gene expression into low and high, surv_cutpoint function of survminer package {Alboukadel Kassambara, Marcin Kosinski and Przemyslaw Biecek (2019). survminer: Drawing Survival Curves using 'ggplot2'. R package version 0.4.6. https://CRAN.R-project.org/package=survminer} was employed.

Additional information on materials

Supplementary Table S2 lists additional information on all materials used in this study.

Quantification and statistical analysis

Sigma Plot version 12.5 was used to perform Unpaired-t tests. Graphpad Prism 8.0 was used for **Two-way ANOVA followed by Bonferroni multiple comparison test. R** was used to perform the Wilcoxon and Logrank test. The statistical details of each experiment can be found in the corresponding figure legend. The replicate number of each experiment was indicated as “n” in the figure legends. For *in vivo* experiments, “n” corresponds to number of animals used in the study. For TCGA analysis, “n” indicates the number of human subjects in a particular group.

Results

Ovarian hormones exhibit growth inhibitory effects on LLC1 tumor cells

The effects of ovarian steroids on LLC1 tumor cells (in terms of cell viability, proliferation and the induction of apoptosis) were first assessed *in vitro*. Controls included incubating cells with either vehicle or cholesterol; viability analysis did not include cholesterol as a control, given it’s known interference with the MTT assay [25]. Both progesterone and estradiol induced a dose-dependent decrease in LLC1 tumor cell viability (Fig. 1A) as well as in proliferative responses (Fig. 1B), compared with relevant controls. A dose-dependent increase in the binding of Annexin-V to LLC1 tumor cells (indicative of apoptosis) was also observed (Fig. 1C). Of note was the fact that progesterone, particularly at higher concentrations, was more effective than estradiol in its effects, both at reducing cell viability and inducing apoptosis. The ability of the two steroids to induce apoptosis was further confirmed by fluorescence microscopy; incubation of LLCl tumor cells with the respective steroids led to enhanced binding of Annexin-V-FITC and propidium iodide, compared with relevant controls (Fig. 1D). Co-incubation of LLC1 tumor cells with sub-optimal doses of both steroids had additive effects on the induction of apoptosis (Fig. 1E). Both steroids therefore display prominent cytocidal effects on LLC1 tumor cells. Studies on A549 cells (a human lung adenocarcinoma cell line) provided further validation of their cytotoxic effects; similar detrimental effects on cell viability (Supplementary Fig. S1A) and proliferation (Supplementary Fig. S1B) were observed.

Progesterone mediates its effects via non-nuclear receptors on LLC1 tumor cells

Further studies focussed on the effects of progesterone because of its greater relevance to subsequent *in vivo* experimentation. At the outset, attempts were made to delineate the receptors responsible for

progesterone action on LLC1 tumor cells. Steroids generally act through their classical/nuclear receptors [26, 27]. Unlike in the ovaries, LLC1 tumor cells however, were found to not express mRNA for the nuclear progesterone receptors Pgr-A or Pgr-B (Fig. 2A). Since steroid-induced expression of nuclear receptors has been described [28], levels of nuclear receptor mRNA were also assessed 24 h post-treatment with progesterone; specific increase over vehicle treatment was not observed (Supplementary Fig. S2). Nevertheless, whether even vehicle-induced increase in nuclear receptors occurring over the course of the experiment could play a role in progesterone-mediated effects was assessed. Mifepristone (a nuclear progesterone receptor antagonist) was unable to reverse the effects of progesterone on LLC1 tumor cell viability (Fig. 2B) or proliferation (Fig. 2C). Taken together, the data strongly suggests that progesterone-mediated cytocidal effects on LLC1 tumor cells are not a consequence of events dependent on the presence of classical/nuclear progesterone receptors.

Several non-nuclear receptors for progesterone have been described [29]. Interestingly, just like the ovaries, LLC1 tumor cells expressed mRNA for several such receptors (Fig. 2D). To assess whether progesterone non-nuclear receptors on LLC1 tumor cells had functional roles, two hallmarks associated with non-classical signalling were evaluated - the activation of mitogen-activated protein (MAP) kinases (described below), and an influence on cAMP levels. Consistent with previous reports [29], the data indicated that progesterone, unlike forskolin, did not induce increases in intracellular cAMP levels in LLC1 tumor cells (Fig. 2E). Assays at varying doses (50 μM, 70 mM) and time points (5 min, 15 min) yielded similar data (not shown). Overall, these experiments led to the conclusion that non-nuclear receptors, and not the nuclear isoforms, are associated with the effects of progesterone on LLC1 tumor cells.

Progesterone-induced cell death is at least partly mediated by activation of p38

Whether MAP kinase pathways were activated in response to signalling via non-nuclear receptors and whether such events were associated with progesterone-induced loss of LLC1 tumor cell viability was then evaluated. Post progesterone incubation, cell lysates were probed with antibodies to phosphorylated and total JNK, ERK, and p38. Interestingly, while the ethanol-containing vehicle induced back-ground phosphorylation of ERK and p38 (albeit with differing kinetics) as also reported in other systems [30], progesterone effectively dampened these effects at most timepoints. Further, analysis of data at 20 min revealed evidence of specific progesterone-induced phosphorylation of JNK and p38. In contrast, progesterone treatment appeared to down-modulate phospho-ERK levels at 20 min (Fig. 3A, B). In order to assign functional relevance to these observations, specific inhibitors for JNK, ERK, and p38 were employed; while phosphorylation of JNK and p38 was once again observed upon progesterone treatment, pre-incubation with the inhibitors resulted in significant inhibitory effects on the phosphorylation of the MAP kinases, as expected (Fig. 3C-E). The viability of cells individually pre-incubated with each inhibitor and subsequently with progesterone was then evaluated by assessing ATP release. While inhibition of ERK and JNK phosphorylation significantly enhanced the loss of viability induced by progesterone (due

to reasons not yet clear), inhibition of p38 phosphorylation significantly ameliorated progesterone-induced cell death to a degree (Fig. 3F).

The activation of MAP kinases confirms the involvement of non-classical signalling via non-nuclear receptors in the growth inhibitory effects of progesterone on LLC1 tumor cells. More specifically, while experimental limitations prevented more effective inhibition of MAP kinase phosphorylation, the data makes evident the involvement of the p38 MAP kinase signalling pathway in the mediation of progesterone-induced cell death.

Characterization of progesterone-induced apoptosis in LLC1 tumor cells

To gain further insight into the nature of progesterone-induced cell death in LLC1 tumor cells, the status of prominent apoptotic mediators was evaluated. Progesterone exposure resulted in an increase in the mRNA levels of Fas, Fas ligand (FasL) as well as BCL-2 antagonist/killer (BAK1); mRNA levels for the BCL-2-associated X protein (BAX) however, remained unchanged (Fig. 4A and B). Evidence of the cleavage of caspase 8 and caspase 9 (both “initiator” caspases) was also obtained upon progesterone exposure. While procaspase 3 (an “executioner” caspase) was also cleaved upon progesterone treatment, caspase 7 (another “executioner” caspase) was not (Fig. 4C). Interestingly, while progesterone induced the up-modulation of apoptosis-related molecules as well as activated the caspase cascade, the pan caspase inhibitor zVAD-fmk could only partially rescue LLC1 tumor cells from progesterone-induced loss of cell viability (Fig. 4D), evidence that alternative mechanisms of cell death could also play a prominent role.

Previous work had established that both hCG [18] and beta-hCG (unpublished data) protect tumor cells from chemotherapeutic agents like tamoxifen (which induces caspase-mediated death [31]), a property that aligns with the fact that cancer patients with high serum beta-hCG levels often respond poorly to chemotherapy [32]. In the present study, while hCG and beta-hCG ameliorated the tamoxifen-induced loss in LLC1 tumor cell viability as expected (Supplementary Fig. S3), neither hCG nor beta-hCG reduced progesterone-induced loss of LLC1 tumor cell viability (Fig. 4E, Supplementary Fig. S3). In line with these observations, progesterone-induced cleavage of caspase 3 was also not prevented by either hCG or beta-hCG (Fig. 4F). While detailed characterization of the pathways of cell death mediated by progesterone in tumor cells is ongoing, these results suggest that, in contrast to when a chemotherapeutic drug is employed, hCG or beta-hCG are unable to mediate cytoprotective effects against the action of progesterone in LLC1 tumor cells.

Progesterone supplementation dampens the enhanced beta-hCG-mediated tumor growth observed in the absence of ovaries in beta-hCG transgenic mice

To assess the *in vivo* responsiveness of LLC1 tumor cells (originally derived from C57BL/6 mice) to progesterone in a milieu containing beta-hCG, transgenic mice of the appropriate genotype were first generated. Wild-type C57BL/6 female mice were outcrossed with heterozygous beta-hCG transgenic ($FVB^{beta\text{-}hCG/-}$) male mice. In female F1 mice, genomic DNA PCR was carried out on tail clips to detect the beta-hCG transgene (Supplementary Fig. S4A), and radioimmunoassay was carried out to detect beta-hCG in serum (Supplementary Fig. S4B). Assessment of body weight (Supplementary Fig. S4C) and serum prolactin (Supplementary Fig. S4D) further distinguished beta-hCG transgenic female mice from non-transgenic littermates, and histological analysis revealed the presence of pituitary adenocarcinomas in transgenic mice (Supplementary Fig. S4E). Ovaries derived from beta-hCG transgenic mice were characterized by hyper-luteinization, whereas ovaries from non-transgenic littermates exhibited normal histology and the presence of follicles at different stages of development (Supplementary Fig. S4F).

At 5-6 months, some transgenic female mice were ovariectomized; decrease in serum prolactin levels (Supplementary Fig. S5) confirmed the efficacy of the procedure. 40,000 LLC1 tumor cells were subcutaneously implanted in non-transgenic mice, transgenic mice, and in ovariectomized transgenic mice; tumor volumes were periodically measured. In keeping with a previous study [33], two key observations were made. Firstly, tumor incidence (Supplementary Fig. S6A) as well as tumor volumes (Supplementary Fig. S6B) were enhanced in beta-hCG transgenic mice compared to non-transgenic littermates. Secondly, ovariectomy led to further enhancement in the growth of LLC1 tumors in ovariectomized beta-hCG transgenic mice, compared with intact beta-hCG transgenic mice (Supplementary Fig. S7).

The effects of progesterone (as well as vehicle) supplementation on the growth of LLC1 tumors in ovariectomized transgenic mice was then assessed. Progesterone efficiently compensated for the absence of ovaries, suppressing the effect of ovariectomy on the growth of LLC1 tumors in beta-hCG transgenic mice (Fig. 5A and B). Significant difference in tumor volumes were not observed in ovariectomized transgenic vehicle-treated mice vs ovariectomized transgenic untreated mice (Supplementary Fig. S8), validating the data described above. At 30 days post-implantation, mice were euthanized and tumors harvested. Excised tumors were subjected to RNA-sequencing and differentially expressed genes (DEGs) were identified by performing DESeq analysis; the two primary comparisons made were between tumors isolated from (1) transgenic (TG) mice vs ovariectomized-TG-vehicle treated (OVX-TG-Veh) mice, and from (2) OVX-TG-Veh mice vs ovariectomized-TG-progesterone treated (OVX-TG-Prog) mice. Gene expressions with a Log2 fold change (>1 or <1) were attributed as upregulated/downregulated respectively. From this gene set, differentially-expressed genes with adjusted P-value of ≤ 0.4 and gene expression value of ≥ 30 were selected (Supplementary Fig. S9). Genes whose expression levels were enhanced upon ovariectomy (in the OVX-TG-Veh gene set) were overlapped with genes whose expression levels declined upon progesterone treatment (in the OVX-TG-Prog gene set), and

vice versa. This approach helped in the identification of putative progesterone-influenced genes that possibly hindered process of LLC1 tumorigenesis. A total of 45 genes - 26 heightened upon ovariectomy and decreased upon progesterone administration, and 19 decreased upon ovariectomy and enhanced upon progesterone administration (Fig. 5C) - were further screened for potential functional significance (using the DAVID database as well as current literature) and genes identified to have an association with tumorigenesis (with described pro- or anti-tumorigenic functions) were selected for validation. Figure 5D depicts a heat map of the selected candidate progesterone-influenced genes, and the mouse figurines at the bottom of the map are indicative of respective tumor volumes in the three experimental conditions compared in the study. Ovariectomy led to an increase in the levels of several pro-tumorigenic genes in LLC1 tumors, the expression of which were down-modulated upon progesterone treatment. Similarly, many anti-tumorigenic genes were down-modulated in these tumors in the absence of the ovaries and up-modulated upon the administration of progesterone. In other words, in these instances, the administration of progesterone had “restorative” effects on mRNA expression of genes associated with tumorigenesis, with levels in tumors isolated from OVX-TG-Prog mice reverting to (and occasionally exceeding) levels in tumors isolated from intact TG mice, mirroring the effect of progesterone administration on LLC1 tumor volumes. Such analysis therefore revealed molecular signatures associated with enhanced beta-hCG-mediated tumorigenesis when the ovaries are absent. The relative expression levels of several RNA-seq-identified genes were validated by qPCR (Fig. 5E and F).

Immunohistochemical analysis was carried out on sections derived from excised tumors to visualize protein products encoded by some of the identified genes. On tumor sections, in several instances, ovariectomy enhanced the expression of proteins classified as “pro-tumorigenic”, and administration of progesterone to ovariectomized transgenic mice reduced the expression to that observed in tumor sections from intact transgenic mice, providing further validation of the steroid’s anti-tumor effects. Curiously, levels of CXCL9 (an “anti-tumorigenic” protein) on tumor sections across the three groups were not in consonance with its mRNA levels as determined both by RNA-seq and qPCR, the reasons for which remain at present unclear. While histological sections depicting these results are shown in Fig. 5G, data is summarized in Supplementary Table S3.

As with LLC1 tumor cells in culture, LLC1 tumors isolated from TG, OVX-TG-Veh or OVX-TG-Prog mice did not express nuclear progesterone receptors, but did express several non-nuclear progesterone receptors, as revealed by both RNA-seq analysis (Supplementary Fig. S10A) as well as semi-quantitative PCR (Supplementary Fig. S10B); mRNA levels did not vary substantially or consistently across the three groups. These results present strong evidence that non-nuclear progesterone receptors mediate the steroid’s anti-tumor effects *in vivo* as well.

It was also of interest to determine if LLC1 tumor cells expressed the conventional LH/CG receptor (the cognate receptor for hCG). Evidence for such expression could not be obtained, either for LLC1 tumor cells grown in culture (Supplementary Fig. S11A), or for tumors excised from the three different groups of mice by RNA-seq analysis (Supplementary Fig. S11B) or by semi-quantitative PCR (Supplementary Fig. S11C). It can be surmised that the actions of beta-hCG in this system are mediated by a moiety other than the conventional LH/CG receptor, the identity of which presently remains unknown.

Progesterone-influenced molecular profile identified by RNA-seq in murine tumors displays clinical relevance

The Cancer Genome Atlas (TCGA) was probed with the tumor-associated progesterone-influenced genes identified in this study, with the ultimate aim of delineating possible relevance of the findings to cancers in post-menopausal women. As previously indicated, this sub-group of women display a higher risk of cancers of different lineages, such as lung adenocarcinoma (LUAD), colorectal adenocarcinoma (COAD) and glioblastoma GBM [2-4]. Hence, TCGA databases for LUAD, COAD and GBM were employed in this study.

Initial analysis, which included subjects from both sexes and all age groups, mapped the human counter parts of genes identified in this study as being potentially influenced by progesterone in beta-hCG transgenic mice. Interestingly, in several instances, the expression patterns of these murine genes overlapped with the expression patterns of their corresponding human orthologs in the TCGA database.

The “anti-tumorigenic genes” TIMP3, TP53INP1 and SFRP2, which were all up-modulated upon progesterone treatment in mice, were also expressed at higher levels in healthy human tissues compared to levels in the three tumor lineages, in a variable manner. Alternatively, “pro-tumorigenic genes” such as LGALS7, MMP10, TNFRSF9, MMP3, MMP12, MMP1, SPP1 and ERO1A (also known as ero1l in mice), down-modulated upon progesterone treatment in transgenic mice, were expressed at higher levels across the three tumor lineages than in healthy tissue, in a variable manner (Fig. 6A, Supplementary Figure S12A and S12B).

Of immediate relevance to this study, several known non-allelic genes encoding beta-hCG (CGB2, CGB3, CGB5, CGB8, and CGB7) were found to be variably up-modulated in COAD and LUAD (Fig. 6A and Supplementary Fig. S12B); the GBM dataset also displayed expression of beta-hCG, albeit at much lower levels (data not shown). TCGA analysis also indicated that LUAD patients with tumors expressing higher amounts of beta-hCG genes (CGB8 and CGB3) have poorer survival compared to patients with tumors

that displayed lower levels of this hormone (data not shown), in line with multiple reports linking tumor-associated beta-hCG with poor patient prognosis.

Interestingly, the expression status of several genes identified in this study demonstrated associations with patient survival, variably across COAD and GBM. For example, high expression levels of CLUSTERIN, FOS, HSPA1B, HSPA1A, TNFRSF9, FOSB (“pro-tumorigenic genes” as per the murine model) correlated with poorer survival, whereas high levels of TP53INP1 and CXCL9 (“anti-tumorigenic genes” as per the murine model) correlated with enhanced survival (Fig. 6B and Supplementary Fig. S13).

Progesterone-influenced molecular profile identified by RNA-seq in murine tumors underscore the onco-protective nature of the pre-menopausal reproductive stratum in women.

The TCGA database was also probed with human orthologs of genes shortlisted in the transgenic model with the menopausal status of women being the qualifier, the logic being that ovariectomy in mice induces a state analogous to the post-menopausal stratum in women. Interestingly, high expression of “pro-tumorigenic gene” (as defined by the transgenic model and enhanced upon ovariectomy) MMP10 in COAD tumors was found to be associated with poor survival only in post-menopausal women but not in pre-menopausal women; while poorer survival was also observed for post-menopausal women harbouring GBM tumors expressing high levels of MMP3, an adequate population of pre-menopausal women expressing high levels of MMP3 in GBM tumors was unavailable for comparison in the database (Fig. 7A and 7B, left and centre panels). Collectively, the data suggested that the impact of these progesterone-influenced genes identified to be “pro-tumorigenic” in ovariectomized transgenic mice on prognosis is similarly dependent upon the presence of a functioning ovary in women.

Whether gene expression levels of the identified progesterone-target genes influenced patient prognosis in pre-menopausal vs post-menopausal women was also assessed by an alternate analysis. High expression of the “pro-tumorigenic gene” (as defined by the transgenic model and enhanced upon ovariectomy) LGALS7 (in COAD) was associated with poor survival specifically in the post-menopausal stratum. Further, high expression of MMP1 (in GBM) and SPP1 (in GBM), other “pro-tumorigenic genes”, was also associated with poorer survival only in post-menopausal women (Fig. 7C). Interestingly, low expression of “pro-tumorigenic genes” such as TNFRSF9, MMP3, and LGALS7 in GBM tumors was also specifically associated with poor prognosis in post-menopausal women (Supplementary Fig. S14A-C). Also, high expression of the “anti-tumorigenic genes” (as defined by the transgenic model and enhanced upon progesterone supplementation) such as CXCL9 (in GBM tumors) displayed corelation with enhanced survival in pre-menopausal women (Fig. 7C).

To summarize, human orthologs of some of the genes identified as “pro-tumorigenic” based on studies in transgenic mice (that is, genes up-modulated in tumors in the absence of ovaries, and down-modulated in tumors upon the administration of progesterone) were preferentially associated with poor prognosis in post-menopausal women, and evidence for the protective effects of “anti-tumorigenic genes” in pre-menopausal group was also obtained. Collectively, these studies outline the onco-protective influence of reproductive hormones in general, and of progesterone in particular.

TCGA analysis revealed several interesting correlates of intra-tumoral beta-hCG with patient prognosis. High expression of CGB3 in LUAD tumors was associated with poorer survival in post-menopausal women (Fig. 7A and 7B, right panels), as was low expression of CGB1 in GBM tumors (Supplementary Fig. S14D).

Discussion

Intra-tumoral hCG / beta-hCG, generally associated with advanced-stage, poorly differentiated cancers, display pro-tumorigenic properties, such as aiding tumor cell invasion [20] and metastasis [21], and is also linked with poor patient prognosis [15, 20, 24, 32, 34–37].

Two additional facts are of direct relevance to this study and its derivative implications: Firstly, several cancers, including glioblastoma, lung cancer and colorectal cancer, occur at an increased frequency in the post-menopausal stratum [2–4]. The increased incidence of cancer observed post-menopause naturally draws attention to the protective influence of female reproductive hormones. In patients with colorectal cancer, better survival in young women (as compared to men of the same age or older women) has been attributed to estradiol [38]. The use of natural progesterone in post-menopausal women is linked with a lower risk of breast cancer [39]. In post-menopausal women, hormonal therapy use has been reported to lower the risk of colorectal cancer [40]. Meta-analysis of colorectal cancer survivors indicated that use of hormone replacement therapy lowers the risk and overall mortality of colorectal cancer in women [41]. Secondly, post-menopausal women, even in the absence of tumors, can display high levels of hCG [6] or beta-hCG [8, 9]. Whether there might exist a cause-effect relationship between these two observations is currently unknown; in other words, the potential role beta-hCG (both intra-tumoral and extra-tumoral) might play in the pathophysiology of cancers in post-menopausal scenarios remains unexplored. The current study was based on testing the hypothesis that ovarian hormones can exert an ameliorating influence on the growth of beta-hCG responsive tumor cells *in vitro* as well as *in vivo*.

In this work, both progesterone and estrogen were shown to negatively impact the growth and survival of LLC1 tumor cells. These cells are derived from granular pneumocytes, equivalent to human alveolar cell carcinoma [42]. The steroids were also shown to have inhibitory effects on the growth of A549 (a human alveolar carcinoma cell line) as well. The inhibitory effects of progesterone, in terms of the migration and invasion of A549 cells, have also been described in other studies [43]; such lineage-associated, cross-

species complementary data increases the relevance of the observations. The anti-tumorigenic effects of ovarian steroids on cancers of different lineages have been previously described as well [44, 45]. While a combination of estradiol and progesterone has been reported to increase proliferation of breast cancer cells [46] and to confer chemoresistance to lung cancer cells [47], the present study suggested additional inhibitory effects on the viability of LLC1 tumor cells upon combination of the two steroids. In line with this observation, combinational hormone replacement therapy with progestogen and estrogen has been shown to be beneficial in the treatment of endometrial cancer [48]. Clearly, the effects of steroid combination therapy appear to be context-dependent, and further investigations are required to unequivocally delineate the conditions under which such therapy would be beneficial.

Going forward, two factors prompted a focus on progesterone, rather than on estradiol, in this study. Firstly, *in vitro* data indicated that progesterone was more potent than estradiol in causing the apoptosis of LLC1 tumor cells, particularly at high doses. Secondly, work by other investigators revealed a significant increase in serum progesterone (and not estradiol) levels with age in beta-hCG transgenic mice [49], an animal model subsequently employed in this work. It was therefore reasoned that studying the biology of progesterone in the context of beta-hCG-mediated tumorigenesis would be appropriate and logical.

Progesterone, while being central to reproductive function, also plays regulatory roles in the functioning of other tissues, including the brain [50], the breast [51], and the bone [52]. Its action primarily involves nuclear progesterone receptor (nPR)-associated classical signaling events. These receptors are known to function as ligand-dependent transcription factors. Two well-characterized isoforms of nPRs exist; PR-A and PR-B [29]. Interestingly, although progesterone mediated significant effects on LLC1 tumor cells in the current study, the cells did not express nuclear progesterone receptors, and neither were such receptors enhanced upon progesterone incubation over levels induced by ethanol, a previously-described property of the vehicle [53]. Experiments employing the nPR antagonist mifepristone further confirmed that the observed effects of progesterone on LLC1 tumor cells were not mediated by nuclear receptors, but possibly via other cognate progesterone receptors.

Recent studies have revealed the identity of several non-nuclear receptors associated with progesterone action in the context of both physiological [54, 55] and pathological [56] conditions. Such receptors include several subtypes of membrane-bound progesterone receptors/progestin and adipoQ receptors (PAQRs), PGRMC1/2, and GABA-A receptors [29]. In the present study, transcripts for several Paqr and Pgrmc receptors were detected in LLC1 tumor cells, and on-going investigations aim at delineating the particular receptor(s) responsible for progesterone action. The progesterone non-nuclear receptor complex is known to act via non-classical mechanisms, including inhibition of adenyl cyclase and cAMP, as well as the activation of MAPKs [29]. Current observations were consistent with previous studies, in that progesterone did not induce an increase in cAMP levels, while it did activate JNK and p38. A lack of progesterone-induced activation of cAMP, as well as activation of JNK and p38 by the steroid, has also been observed in human ovarian cancer cells, effects also attributed to non-nuclear receptors [57].

MAPKs have well-established roles in modulating apoptosis [58]. p38 has been documented to have pro-apoptotic functions [59], including activation of caspase-3 [60], and progesterone induces apoptosis in HUVECs via p38 [61]. p38 activation via progesterone-mPR complex has also been proposed to induce apoptosis of ovarian cancer cells [62]. Supportive of these reports, the present study demonstrates that inhibiting progesterone-induced activation of p38 can lead to the partial rescue of LLC1 tumor cells from death. Given this data, it can be surmised that progesterone induces apoptosis in LLC1 tumor cells at least partially via the activation of p38 pathway subsequent to triggering of the progesterone-mPR complex.

Observations in beta-hCG transgenic mice provided critical insights into the cytopathic effects of progesterone in a beta-hCG-containing milieu. RNA-seq analysis on excised tumors helped reveal the nature of genes that are modulated both by ovariectomy and by progesterone supplementation in beta-hCG transgenic mice. Differential gene expression analysis revealed that the mRNA levels of “anti-tumorigenic genes” such as Timp3, Sulf1, Trp53inp1, Sfrp2, and Ptpn13 (all with well-described pro-apoptotic functions) were diminished upon ovariectomy and enhanced upon progesterone administration. Though progesterone also induced activation of both initiator and executioner caspases in LLC1 tumor cells *in vitro*, data suggests that progesterone-induced cell death may predominantly involve caspase-independent mechanisms, since a pan-caspase inhibitor was only partially effective in rescuing cells from death. Interestingly, TP53INP1 (the human ortholog of mouse Trp53inp1) is also known to induce autophagy-dependent cell death [63]. Autophagy, originally described as a cell rescue program, can also initiate cell death [64], either acting independently or in conjunction with apoptosis and other regulatory cell death mechanisms [64, 65]. Pharmacological interventions that aid apoptosis [66] or associated regulatory cell death mechanisms such as pro-death function of autophagy [67] in tumors have been considered promising and efficient strategies to target cancer cells. Whether autophagy is indeed involved in the induction of LLC1 tumor cell death by progesterone is currently unknown but is worth exploring.

As with any work, it is important to put the observations into perspective from a human context. According to the GLOBOCAN Cancer Tomorrow Prediction Tool, the estimated number of new cancer cases and deaths in women in the 55–85 + age group are expected to increase by 58% and 70% respectively in the next twenty years. In order to aid in the efficient clinical management of these patients, a better understanding of the post-menopausal state therefore remains an exigency. This study provides some clues in this regard.

Intra-tumoral beta-hCG has traditionally been considered an indicator of poor patient prognosis. Interestingly, TCGA analysis revealed that beta-hCG expression (CGB3 in LUAD patients and the CGB1 in GBM patients) displayed association with poorer survival in post-menopausal women, indicating its presence could have a special pathological significance in this cohort.

Several beta-hCG driven, progesterone-influenced genes identified in this work are known to play critical roles in the progression of human cancer. Genes such as SPP1, MMP3, MMP1, MMP12, LGALS7, ERO1A,

TNFRSF9 identified as “pro-tumorigenic” in the murine model, are expressed at higher levels in human tumors; these genes are known to influence the processes of proliferation, migration, invasion and/or chemoresistance resistance in tumor cells.

Perhaps more significantly, a gene signature identified in this study demonstrated prognostic relevance in cancers particularly associated with the post-menopausal state. In several instances, TCGA analysis revealed the association of the expression of progesterone-influenced “pro-tumorigenic genes” with poor prognosis, specifically in post-menopausal cancer patients; examples include MMP10, LGALS7 in COAD, and MMP1, SPP1, TNFRSF9, MMP3 and LGALS7 in GBM. The degree of molecular overlap between tumor behavior in ovariectomized beta-hCG transgenic mice and in post-menopausal women is interesting and instructive.

The expression of non-nuclear progesterone receptors seems fairly ubiquitous in tumor cells [29, 56, 57]. As with LLC1 tumor cells in culture, tumors from beta-hCG transgenic mice too exclusively expressed non-nuclear progesterone receptors. Further, TCGA analysis revealed that GBM, LUAD and COAD human tumors also exclusively express non-nuclear receptors for progesterone; while LUAD tumors derived from post-menopausal women category express only PAQR6, COAD tumors from these women displays high levels of PGRMC1,2 and PAQR 3,4,5,7,8, while nuclear progesterone receptor expression is insignificant. Also, GBM tumors from these women express higher levels of PGRMC1 and PAQR 6,8, with low expression of PAQR9 (Supplementary Fig. S15). Whether the presence of such receptors presents a therapeutic opportunity remains an open question.

The principal findings and their implications have been summarized and represented in Fig. 8.

Conclusions

This study identifies, for the first time, the inter-relationship between progesterone and beta-hCG in regulating the process of neoplastic transformation. It associates a previously unidentified negative attribute to beta-hCG specifically in the post-menopausal state, while also demonstrating the tumor-suppressing effects of progesterone both *in vitro* and *in vivo*. Significantly, several newly-identified, beta-hCG driven, progesterone-influenced genes, revealed correlates with prognosis, specifically in post-menopausal women harboring aggressive cancers. Correlation of intra-tumoral beta-hCG with poorer survival in post-menopausal women, along with data presented in this paper makes the case for the evaluation of both extra-tumoral and intra-tumoral beta-hCG as prognostic indicators in tumor-bearing, post-menopausal women.

Beta-hCG did not ameliorate the cytotoxic effects of progesterone on tumor cells, unlike its protective effects against conventional chemotherapeutic drugs, as this study and previous work [18, 68, 69] has shown. The inability of beta-hCG to dampen the cytocidal effects of progesterone could be a useful therapeutic attribute, particularly if the steroid were employed in conjunction with anti-hCG vaccination which has demonstrated, albeit partial, anti-tumor efficacy in several murine systems [18, 19, 70 71–73]

and in humans [74]. The fact that non-nuclear progesterone receptors are preferentially present on tumors isolated from post-menopausal women is a significant factor in favor of such approaches.

The extent of overlap between genes identified in the murine model and their human orthologs as regards potential roles in the ovary deficient / inactive state encourages use of the model in future investigations seeking to delineate the interplay between chorionic gonadotropin and steroid hormones in the process of tumorigenesis in lineages of particular relevance to the post-menopausal state.

Declarations

Ethics approval

All animal studies were performed in compliance with the U.S. Department of Health and Human Services Guide for the Care and Use of Laboratory Animals. In addition, this study was carried out in accordance with the recommendations of the Committee for the Purpose of Control and Supervision of Experiments on Animals (CPCSEA), Government of India. The protocol was approved by the institutional animal ethics committee of the National Institute of Immunology (IAEC#528/19).

Consent for publication

Not applicable

Availability of data and materials

Data generated or analysed during this study and information on all materials are included in the manuscript and the “Supplementary information_additional materials” file. RNA-seq raw and processed data have been deposited at GEO (accession number: GSE186999) and are publicly available as on the date of publication. Raw data for Western blots (“BLOTS_raw data) and agarose gels (“AGAROSE GELS_raw data”) has been provided.

Competing interests

All authors declare no conflict of interests.

Funding

This work was support by an extramural grant from the Department of Biotechnology, Government of India (Grant Number: BT/PR20822/MED/30/1726/2016) and by core grants to the National Institute of Immunology, New Delhi India.

Authors' contributions

M.S. and R.P. conceptualized the study, decided on methodology and wrote the manuscript; M.S. carried out most experimentation; R.D.S., H.S. and M.S. carried out TCGA analysis; P.S. and M.S. carried out ovariectomies and follow-up; U.A. and R.R. conducted the histochemical analysis; M.S., R.D.S., U.A. and R.P. carried out formal analysis; R.D.S, U.A. and R.P. contributed resources; R.P. supervised the study.

Acknowledgments

We thank Dr. P. Nagarajan and Mr. Shailendra Kumar Arindkar for discussions on the protocols for the isolation of genomic DNA and Mr. Animesh Kar for help with RNA-seq data analysis. Beta-hCG transgenic mice were a kind gift from Dr. Ilpo Huhtaniemi, Imperial College, UK. The graphical abstract was created using BioRender.com.

Supplementary Information / Additional Materials

File name: Supplementary Information_Additional Materials

File format: PDF

File Content: Supplementary Figures (S1- S15), Supplementary Tables (S1-S3).

References

1. Dalal PK, Agarwal M. Postmenopausal syndrome. Indian J. Psychiatry. 2015; 57:S222-S232.
2. Min L, Wang F, Liang S, Yang J, Xu X. Menopausal status and the risk of lung cancer in women: A PRISMA-compliant meta-analysis. Medicine(Baltimore).2017;96:e7065.
3. Franceschi S, Gallus S, Talamini R, Tavani A, Negri E, La Vecchia C. Menopause and colorectal cancer. Br. J. Cancer. 2000;82:1860-1862.
4. Huang K, Whelan EA, Ruder AM, Ward EM, Deddens JA, Davis-King KE, et al. Reproductive factors and risk of glioma in women. Cancer Epidemiol. Biomarkers Prev. 2004;13:1583-1588.
5. Surakasula A, Nagarjunapu GC, Raghavaiah KV. A comparative study of pre- and post-menopausal breast cancer: Risk factors, presentation, characteristics and management. J. Res. Pharm. Pract.

2014;3:12-18.

6. Snyder JA, Haymond S, Parvin CA, Gronowski AM, Grenache DG. Diagnostic considerations in the measurement of human chorionic gonadotropin in aging women. Clin.Chem. 2005;51:1830-1835.
7. Hage LE, Hatipoglu B. Elevated hCG can be a benign finding in perimenopausal and postmenopausal women. Cleve. Clin. J. Med. 2021;88: 635-639.
8. Bashir I, Ihenetu K, Miller JJ, Gim M-H, Lippmann S. A positive pregnancy test in the post-menopausal psychiatric patient-: what to think?. Psychiatry (Edgmont). 2006;3:58-60.
9. Daiter E, Braunstein GD, Snyder PJ, Coutifaris C, Mastroianni L Jr, Pavlou SN, et al. Gonadotropin-releasing hormone-dependent chorionic gonadotropin secretion in a menopausal woman. J. Clin. Endocrinol. Metab. 1994;78:1293-1297.
10. Surampudi K, Gundabattula SR. The role of serum beta hCG in early diagnosis and management strategy of ectopic pregnancy. J. Clin. Diagn. Res. 2016;10:QC08-QC10.
11. Dieckmann KP, Simonsen-Richter H, Kulejewski M, Anheuser P, Zecha H, Isbarn H, et al. Serum tumour markers in testicular germ cell tumours: frequencies of elevated levels and extents of marker elevation are significantly associated with clinical parameters and with response to treatment. Biomed. Res. 2019;5030349. Int. doi: 10.1155/2019/5030349.
12. Jagtap SV, Aher V, Gadhiya S, Jagtap SS. Gestational trophoblastic disease - clinicopathological study at tertiary care hospital. J. Clin. Diagn. Res. 2017;11: EC27-EC30.
13. Iles RK, Purkis PE, Whitehead PC, Oliver RT, Leigh I, Chard T. Expression of beta human chorionic gonadotrophin by non-trophoblastic non-endocrine 'normal' and malignant epithelial cells. Br. J. Cancer. 1990;61:663-666.
14. Nakanuma Y, Unoura M, Noto H, Ohta G. Human chorionic gonadotropin in primary liver carcinoma in adults. Virchows Archiv A. 1986;409:365-373.
15. Yamaguchi A, Ishida T, Nishimura G, Kumaki T, Katoh M, Kosaka T, et al. Human chorionic gonadotropin in colorectal cancer and its relationship to prognosis. Br. J. Cancer. 1989;60:382-384.
16. Wong YP, Tan GC, Aziz S, Pongprakyun S, Ismail F. Beta-human chorionic gonadotropin-secreting lung adenocarcinoma. Malays. J. Med. Sci. 2015;22: 76-80.
17. Cole LA. HCG variants, the growth factors which drive human malignancies. Am. J. Cancer Res. 2012;2:22-35.
18. Sahoo S, Singh P, Kalha B, Singh O, Pal R. Gonadotropin-mediated chemoresistance: Delineation of molecular pathways and targets. BMC Cancer. 2015;15.
19. Khare P, Bose A, Singh P, Singh S, Javed S, Jain SK, et al. Gonadotropin and tumorigenesis: Direct and indirect effects on inflammatory and immunosuppressive mediators and invasion. Mol. Carcinog. 2016;56:359-370.
20. Li J, Yin M, Song W, Cui F, Wang W, Wang S, et al. B subunit of human chorionic gonadotropin promotes tumor invasion and predicts poor prognosis of early-stage colorectal cancer. Cell. Physiol. Biochem. 2018;45:237-249.

21. Wu W, Gao H, Li X, Peng S, Yu J, Liu N, et al. β-hCG promotes epithelial ovarian cancer metastasis through ERK/MMP2 signaling pathway. Cell Cycle. 2019;18:46-59.
22. Hameed A, Miller DS, Muller CY, Coleman RL, Albores-Saavedra J. Frequent expression of beta-human chorionic gonadotropin (beta-hCG) in squamous cell carcinoma of the cervix. Int. J. Gynecol. Pathol. 1999;18:381-386.
23. Guo X, Liu G, Schauer IG, Yang G, Mercado-Uribe I, Yang F, et al. Overexpression of the β subunit of human chorionic gonadotropin promotes the transformation of human ovarian epithelial cells and ovarian tumorigenesis. Am. J. Pathol. 2011;179:1385-1393.
24. Venyo AK-G, Herring D, Greenwood H, Maloney DJL. The expression of beta human chorionic gonadotrophin (β-HCG) in human urothelial carcinoma. Pan. Afr. Med. 2010;7:20.
25. Ahmad S, Ahmad A, Schneider KB, White CW. Cholesterol interferes with the MTT assay in human epithelial-like (A549) and endothelial (HLMVE and HCAE) cells. Int. J. Toxicol. 2006;25:17-23.
26. Jacobsen BM, Horwitz KB. Progesterone receptors, their isoforms and progesterone regulated transcription. Mol.Cell.Endocrinol. 2012;357:18-29.
27. Lösel R, Wehling M. Nongenomic actions of steroid hormones. Nat. Rev. Mol. Cell Biol. 2003;4:46-55.
28. Diep CH, Ahrendt H, Lange CA. Progesterone induces progesterone receptor gene (PGR) expression via rapid activation of protein kinase pathways required for cooperative estrogen receptor alpha (ER) and progesterone receptor (PR) genomic action at ER/PR target genes. Steroids. 2016;114:48-58.
29. Garg D, Ng SSM, Baig KM, Driggers P, Segars J. Progesterone-mediated non-classical signaling. Trends Endocrinol. Metab. 2017;28:656-668.
30. Ku BM, Lee YK, Jeong JY, Mun J, Han JY, Roh GS. Ethanol-induced oxidative stress is mediated by p38 MAPK pathway in mouse hippocampal cells. Neurosci. Lett. 2007;419:64-67.
31. Mandlekar S, Yu R, Tan TH, Kong AN. Activation of caspase-3 and c-Jun NH2-terminal kinase-1 signaling pathways in tamoxifen-induced apoptosis of human breast cancer cells. Cancer Res. 2000;60:5995-6000.
32. Szturmowicz M, Wiatr E, Sakowicz A, Slodkowska J, Roszkowski K, Filipecki S, et al. The role of human chorionic gonadotropin beta subunit elevation in small-cell lung cancer patients. J. Cancer Res. Clin. Oncol. 1995;121:309-312.
33. Singh P, Sarkar M, Agrawal U, Huhtaniemi I, Pal R. The transgenic expression of the β-subunit of human chorionic gonadotropin influences the growth of implanted tumor cells. Oncotarget. 2018;9:34670-34680.
34. Sheaff MT, Martin JE, Badenoch DF, Baithun SI. Beta hCG as a prognostic marker in adenocarcinoma of the prostate. J Clin Pathol. 1996;49:329–332.
35. Crawford RA, Iles RK, Carter PG, Caldwell CJ, Shepherd JH, Chard T. The prognostic significance of human chorionic gonadotrophin and its metabolites in women with cervical carcinoma. J Clin Pathol. 1998;51:685-688.

36. Iles R, Persad KR Trivedi M, Sharma KB, Dickinson A, Smith P et al. Urinary concentration of human chorionic gonadotrophin and its fragments as a prognostic marker in bladder cancer. Br J Urol. 1996;77:61-69.
37. Douglas J, Sharp A, Chau C, Head J, Drake T, Wheater M et al. Serum total hCGβ level is an independent prognostic factor in transitional cell carcinoma of the urothelial tract. Br J Cancer. 2014;110:1759-1766.
38. Abancens M, Bustos V, Harvey H, McBryan J, Harvey BJ. Sexual dimorphism in colon cancer. Front. Oncol. 2020;10:607909.
39. Lieberman A, Curtis L. In defense of progesterone: A review of the literature. Altern. Ther. Health Med. 2017;23:24-32.
40. Botteri E, Støer NC, Sakshaug S, Graff-Iversen S, Vangen S, Hofvind S, et al. Menopausal hormone therapy and colorectal cancer: a linkage between nationwide registries in Norway. BMJ Open. 2017;7:e017639.
41. Jang Y-C, Huang H-L, Leung CY. Association of hormone replacement therapy with mortality in colorectal cancer survivor: a systematic review and meta-analysis. BMC Cancer. 2019;19:1199.
42. Garcia-Sanz M, Simón-Marín R, Hilario E. Morphological characterization of Lewis lung carcinoma (3LL). A light and electron microscopic study. Tumori. 1989;75:23-27.
43. Xie M, You S, Chen Q, Chen X, Hu C. Progesterone inhibits the migration and invasion of A549 lung cancer cells through membrane progesterone receptor α-mediated mechanisms. Oncol. Rep. 2013;29:1873-1880.
44. Lee S, Lee M, Kim JB, Jo A, Cho EJ, Yu SJ, et al. 17β-estradiol exerts anticancer effects in anoikis-resistant hepatocellular carcinoma cell lines by targeting IL-6/STAT3 signaling. Biochem. Biophys. Res. Commun. 2016;473:1247-1254.
45. Wu NY, Huang HS, Chao TH, Chou HM, Fang C, Qin CZ, et al. Progesterone prevents high-grade serous ovarian cancer by inducing necroptosis of p53-defective fallopian tube epithelial cells. Cell Rep. 2017;18:2557-2565.
46. Tian JM, Ran B, Zhang CL, Yan DM, Li XH. Estrogen and progesterone promote breast cancer cell proliferation by inducing cyclin G1 expression. Braz. J. Med. Biol. Res. 2018;51:1-7.
47. Grott M, Karakaya S, Mayer F, Baertling F, Beyer C, Kipp M, et al. Progesterone and estrogen prevent cisplatin-induced apoptosis of lung cancer cells. Anticancer Res. 2013;33:791-800.
48. Mayor S. Continuous HRT with oestrogen plus progestogen is linked to reduced risk of endometrial cancer. BMJ. 2015;351:h6627.
49. Rulli SB, Kuorelahti A, Karaer O, Pelliniemi LJ, Poutanen M, Huhtaniemi I. Reproductive disturbances, pituitary lactotrope adenomas, and mammary gland tumors in transgenic female mice producing high levels of human chorionic gonadotropin. Endocrinology. 2002;143:4084-4095.
50. Brinton RD, Thompson RF, Foy MR, Baudry M, Wang J, Finch CE, et al. Progesterone receptors: form and function in brain. Front. Neuroendocrinol. 2008;29:313-339.

51. Druckmann R. Progestins and their effects on the breast. Maturitas. 2003;46: 59-69.
52. Seifert-Klauss V, Prior JC. Progesterone and bone: actions promoting bone health in women. J. Osteoporos. 2010;845180.
53. Etique N, Flament S, Lecomte J, Grillier-Vuissoz I. Ethanol-induced ligand-independent activation of ERalpha mediated by cyclic AMP/PKA signaling pathway: an in vitro study on MCF-7 breast cancer cells. Int. J. Oncol. 2007;31:1509-1518.
54. Gellersen B, Fernandes MS, Brosens JJ. Non-genomic progesterone actions in female reproduction. Hum. Reprod. Update. 208;15:119-138.
55. Singh M, Su C, Ng S. Non-genomic mechanisms of progesterone action in the brain. Front. Neurosci. 2013;7:159.
56. Pedroza DA, Subramani R, Lakshmanaswamy R. Classical and non-classical progesterone signaling in breast cancers. Cancers (Basel). 2020;12:2440.
57. Charles NJ, Thomas P, Lange CA. Expression of membrane progesterone receptors (mPR/PAQR) in ovarian cancer cells: implications for progesterone-induced signaling events. Horm. Cancer. 2010;1:167-176.
58. Yue J, López JM. Understanding MAPK signaling pathways in apoptosis. Int. J. Mol. Sci. 2020;21:2346.
59. Dolado I, Swat A, Ajenjo N, De Vita G, Cuadrado A, Nebreda AR. p38α MAP Kinase as a sensor of reactive oxygen species in tumorigenesis. Cancer Cell. 2007;11:191-205.
60. Pearl-Yafe M, Halperin D, Scheuerman O, Fabian I. The p38 pathway partially mediates caspase-3 activation induced by reactive oxygen species in Fanconi anemia C cells. Biochem. Pharmacol. 2004;67:539-546.
61. Powazniak Y, Kempfer AC, de la Paz Dominguez M, Farias C, Keller L, Calderazzo JC, et al. Effect of estradiol, progesterone and testosterone on apoptosis- and proliferation-induced MAPK signaling in human umbilical vein endothelial cells. Mol. Med. Rep. 2009;2:441-447.
62. Valadez-Cosmes P, Vázquez-Martínez ER, Cerbón M,Camacho-Arroyo I. Membrane progesterone receptors in reproduction and cancer. Mol. Cell. Endocrinol. 2016;434:166-175.
63. Shahbazi J, Lock R, Liu T. Tumor protein 53-induced nuclear protein 1 enhances p53 function and represses tumorigenesis. Front. Genet. 2013;4.
64. Gozuacik D, Kimchi A. Autophagy as a cell death and tumor suppressor mechanism. Oncogene. 2004;23:2891-2906.
65. Noguchi M, Hirata N, Tanaka T, Suizu F, Nakajima H, Chiorini JA. Autophagy as a modulator of cell death machinery. Cell Death Dis. 2020;11:517.
66. Pfeffer CM, Singh ATK. Apoptosis: A target for anticancer therapy. Int. J. Mol. Sci. 2018;19:448.
67. Linder B, Kögel D. Autophagy in cancer cell death. Biology (Basel). 2019;8:82.
68. You B, Pollet-Villard M, Fronton L, Labrousse C, Schott A-M, Hajri T et al. Predictive values of hCG clearance for risk of methotrexate resistance in low-risk gestational trophoblastic neoplasias. Ann

Oncol. 2010;21:1643-1650.

69. Kuroda H, Mandai M, Konishi I, Yura Y, Tsuruta Y, Hamid AA et al. Human chorionic gonadotropin (hCG) inhibits cisplatin-induced apoptosis in ovarian cancer cells: Possible role of up-regulation of insulin-like growth factor-1 by hCG. Int J Cancer. 1998;76:571-578.
70. Sachdeva R, Bhardwaj N, Huhtaniemi I, Aggrawal U, Jain SK, Zaidi R, et al. Transgenesis-mediated reproductive dysfunction and tumorigenesis: Effects of immunological neutralization. PLOS ONE. 2012;7:e51125.
71. Bose A, Huhtaniemi I, Singh O, Pal R. Synergistic activation of innate and adaptive immune mechanisms in the treatment of gonadotropin-sensitive tumors. PLOS ONE. 2013;8:e61288.
72. Acevedo HF, Raikow RB, Powell JE, Stevens VC. Effects of immunization against human choriogonadotropin on the growth of transplanted Lewis lung carcinoma and spontaneous mammary adenocarcinoma in mice. Cancer Detect Prev Suppl. 1987;1:477–486.
73. Jiang C, Jiang Y, Huang Z, Shen W, Wang J, Shen Q. Evaluation of the immunogenicity of a single chain chimeric peptide composed of hCGb and oLHa for inhibition of the growth of hCGb-expressing cancer cells. Cancer Immunol Immunother. 2010;59:1771–1779.
74. Moulton HM, Yoshihara PH, Mason DH, Iversen PL, Triozzi PL. Active specific immunotherapy with a β-Human Chorionic Gonadotropin peptide vaccine in patients with metastatic colorectal cancer: antibody response is associated with improved survival. Clin. Cancer Res. 2002;8:2044-2051.

Figures

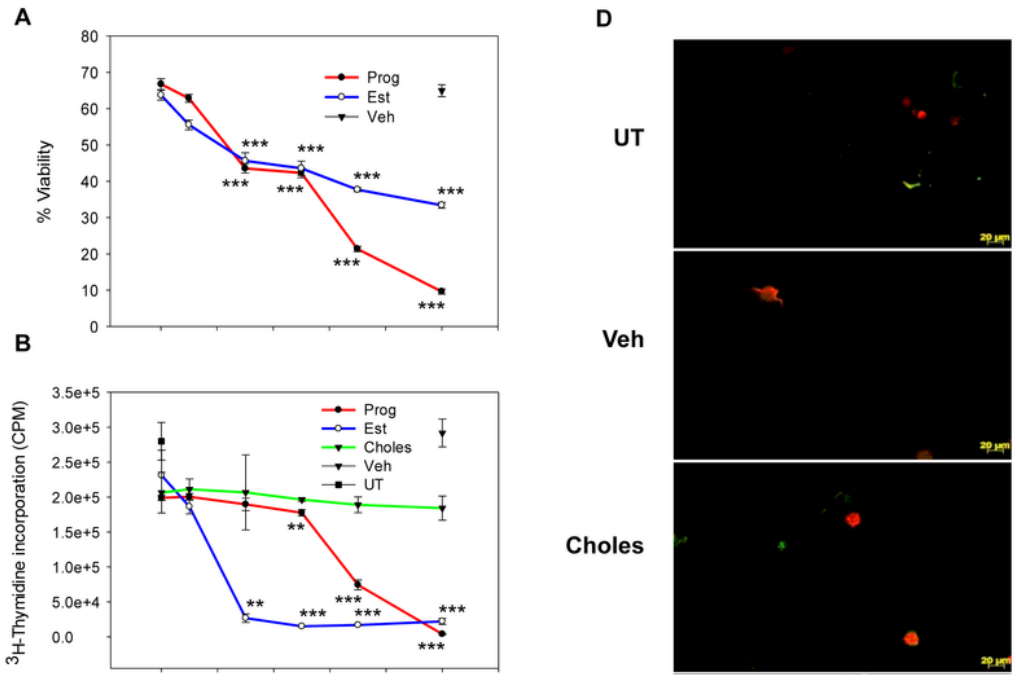

Figure 1

Ovarian hormones exhibit growth inhibitory effects on LLC1 tumor cells

(A) LLC1 tumor cells were incubated with varying concentrations (0.1-100 μM) of Progesterone (Prog) or Estradiol (Est) for 48 h. Veh: Vehicle (ethanol). Cell viability was assessed by MTT. Data is plotted as percentage viability over untreated cells. Values represent arithmetic mean ± SD **(n=3). Each value compared to highest concentration of Veh. ***p<0.001** by the Unpaired t-test.

(B) Experimental setup identical to Fig. 1A. Proliferation was assessed by measuring the incorporation of ^{3}H-thymidine. Values represent arithmetic mean ± SD (n=3). Each value was compared with corresponding values of the negative control Cholesterol (Choles). **p<0.01, ***p<0.001 by the Unpaired t-test. UT: Untreated cells.

(C) Experimental setup identical to Fig. 1A. Annexin-V expression was assessed by flow cytometry. Values represent arithmetic mean ± SD (n=3). Each value was compared with corresponding values of the negative control (Choles). *p<0.05, **p<0.01, ***p<0.001 by the Unpaired t-test.

(D) Fluorescence images of LLC1 tumor cells incubated with respective steroids (50 μM) for 24 h and then stained with Annexin-V-FITC and propidium iodide.

(E) LLC1 tumor cells were individually incubated with Prog, Est or Choles (30 μM), or with the indicated combinations, for 48 h. Annexin-V expression was assessed by flow cytometry. Values represent arithmetic mean ± SD (n=3). *p<0.05, **p<0.01 by the Unpaired t-test.

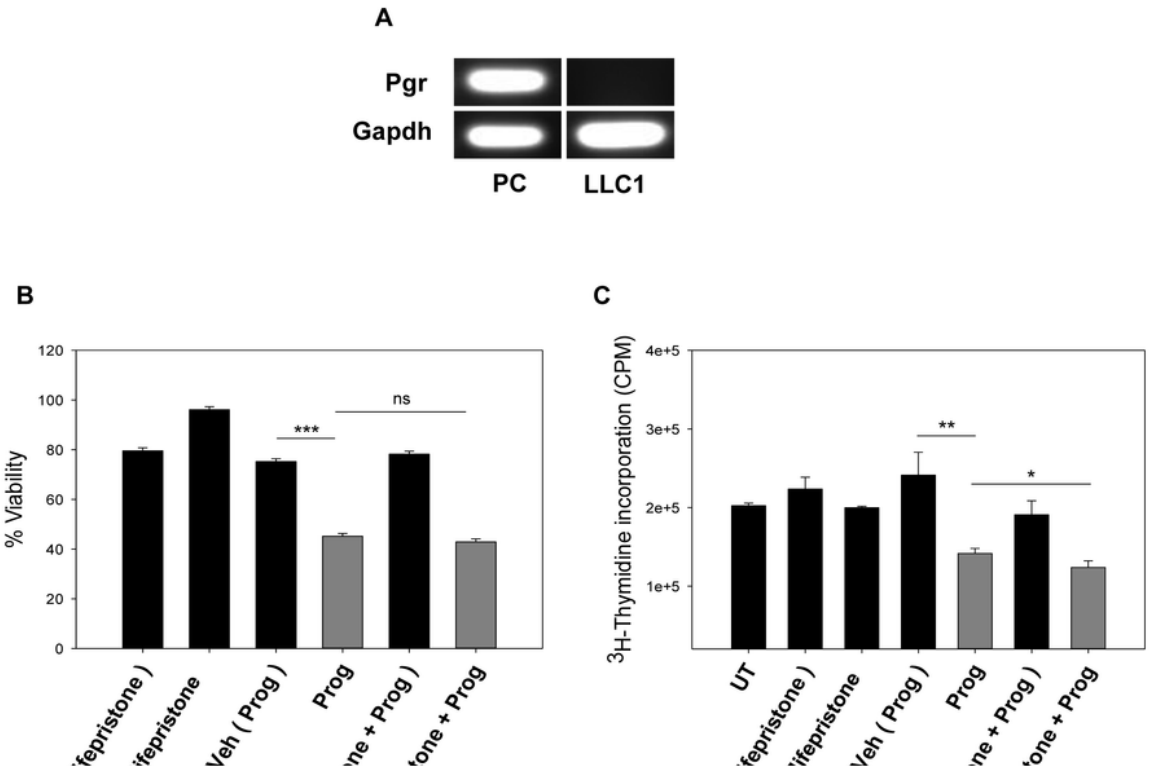

Figure 2

Progesterone mediates its effects via non-nuclear receptors on LLC1 tumor cells

(A) Expression of the mRNA for Progesterone nuclear receptor (Pgr) in LLC1 tumor cells. 1 µg of total RNA was reverse transcribed to cDNA, and PCR carried out. mRNA from BALB/c ovaries, employed as positive control (PC). The primer employed (sequence provided in TABLE S2) amplifies both isoforms (A and B) of Pgr. The vertical gap between the bands denotes missing wells in the gel (raw data provided).

(B) LLC1 tumor cells were incubated with Mifepristone (500 nM) for 12 h followed by incubation with Prog (50 mM) for 48 h. Veh (Mifepristone): DMSO; Veh (Mifepristone+Prog): DMSO+ethanol. **Cell viability was assessed by MTT. Data is plotted as percentage viability over untreated cells. Values represent arithmetic mean ± SD (n=3). ***p<0.001 by the Unpaired t-test. ns: non-significant.**

(C) Experimental set-up similar to (B). **Proliferation was assessed by measuring the incorporation of ^{3}H-thymidine. Values represent arithmetic mean ± SD (n=3). *p<0.05, **p<0.01 by the Unpaired t-test.**

(D) Expression of mRNA for non-nuclear progesterone receptors in LLC1 tumor cells. mRNA from BALB/c ovaries, employed as positive control (PC). 1 µg of total RNA was reverse transcribed to cDNA, and PCR carried out. The vertical gap between the bands denotes missing wells in the gels (raw data provided).

(E) LLC1 tumor cells were incubated with phosphodiesterase inhibitors IBMX and Ro-20-1724 for 30 min prior to incubation with Forskolin (100 mM/10 min) or Prog (100 mM/30 min). Veh (Forskolin): DMSO. A luminescence-based assay for cAMP was then performed. Each luminescence (RLU) value was normalized to blank. Concentrations were calculated using four-parameter logistic curve regression model. **Values represent arithmetic mean ± SD (n=2). Value compared to respective vehicles. ***p<0.001 by the Unpaired t-test.**

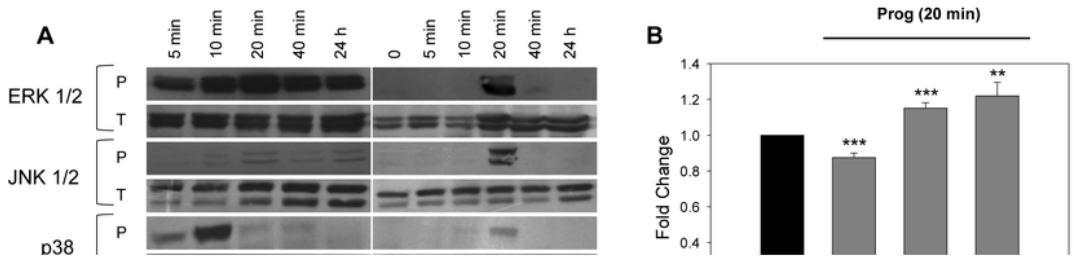

Figure 3

Progesterone-induced cell death is at least partly mediated by activation of p38

(A) LLC1 tumor cells were incubated with Prog (50 μM) or the Veh for the indicated timepoints. Lysates were then assessed for evidence of MAPK activation by Western blot. The vertical gaps between the data for Veh and Prog for each antibody indicates separate blots; blots were exposed to the same X-ray film to ensure equal exposure to chemiluminescent signals (raw data provided). Gapdh for one representative experiment is shown. Data for pJNK, JNK, Gapdh (Veh and Prog), phospho-p38 (Prog) and p38 (Prog) are mirror images of the original (raw data provided). Densitometry was performed on raw data.

(B) Densitometry analysis of data in (A). Each phospho (P) band at 20 min was normalized to its corresponding band indicating total (T) reactivity. Fold change in phosphorylation (Prog vs Veh) at 20 min is represented. Values represent arithmetic mean fold change ± SD (n=3). **p<0.01, ***p<0.001 by the Unpaired t-test.

(C) LLC1 tumor cells were incubated with inhibitors (i) for ERK (PD98059), JNK (JNK II inhibitor), or p38 (SB203580) (20 mM) for 1 hr followed by treatment with Prog (50 mM) for 20 min. Veh (i + Prog): DMSO + ethanol. Lysates were then assessed for evidence of MAPK activation by Western blot. Gapdh for one representative experiment is shown. The Prog and Veh (Prog) data for Gapdh have been used across this data since they represent identical samples from the same experiment.

(D) Densitometry analysis of data in (C). Each phospho (P) band was normalized to its corresponding band indicating total (T) reactivity. Fold change in phosphorylation (Prog vs Veh) at 20 min is represented. Values represent arithmetic mean fold change ± SD (n=3). *p<0.05, ***p<0.001 by the Unpaired t-test.

(E) Densitometry analysis of data in (C). Each phospho (P) band was normalized to its corresponding band indicating total (T) reactivity. Fold change in phosphorylation (i + Prog vs Prog) at 20 min is represented. Values represent arithmetic mean fold change ± SD (n=3). *p<0.05, ***p<0.001 by the Unpaired t-test.

(F) LLC1 tumor cells were pre-incubated with indicated inhibitors (i, 20 μM) for 1 h followed by treatment with Prog (15 mM) for 24 h. Intracellular ATP was measured to assess cell viability. Data is plotted as percentage viability over untreated cells. Values represent arithmetic mean ± SD (n=3). ***p<0.001 by the Unpaired t-test.

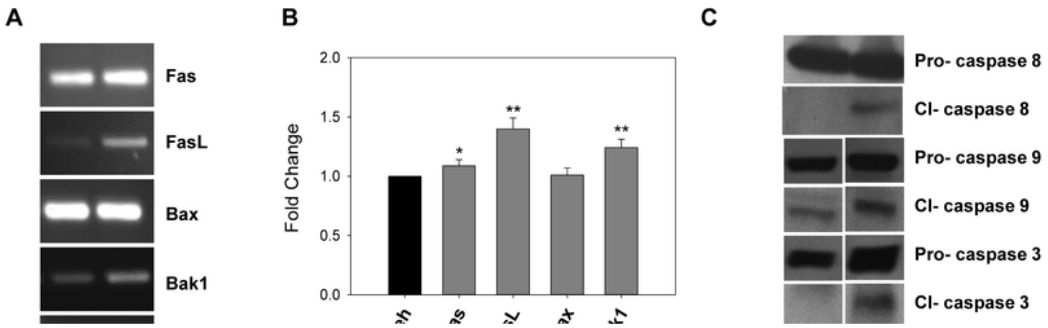

Figure 4

Characterization of progesterone-induced apoptosis in LLC1 tumor cells

(A) LLC1 tumor cells were incubated with Veh or Prog (50 mM) for 24 h. 1 µg of total RNA was reverse transcribed to cDNA, and PCR for the **indicated genes were** carried out**. Gapdh for the same experiment is shown. Each image is a mirror image of the original lanes in gel (raw data provided).**

(B) Densitometry analysis of data in (A). Band intensities were normalized to respective Gapdh controls. Fold change in expression in Prog vs Veh treatment is shown. Values represent arithmetic mean fold change ± SD (n=3). *p<0.05, **p<0.01 by Unpaired t-test.

(C) LLC1 tumor cells were incubated with Veh or Prog (50 µM) for 24 h. Lysates were then assessed for evidence of caspase activity by Western blot, employing antibodies to indicated caspases (pro and cleaved-Cl). The vertical gap between the blots for caspases 3 and 9 implies missing bands within a blot (for caspase 3) or separate blots (for caspase 9) and the horizontal gap for a given caspase denotes splitting of the same blot to efficiently capture pro- and cleaved fragments separately. Blots were exposed to the same X-ray film to ensure equal exposure to chemiluminescent signals (raw data provided). Caspase-8 (pro and cleaved) are mirror images of the raw data. Gapdh (mirror image of original data) for one representative experiment is shown.

(D) LLC1 tumor cells were co-incubated with a pan-caspase inhibitor (zVAD, 75 or 100 µM) and Prog (10 µM) for 24 h. Veh (zVAD): DMSO; Veh (zVAD + Prog): DMSO + ethanol. Intracellular ATP was measured to assess cell viability. Data is plotted as percentage viability over untreated cells. Values represent arithmetic mean ± SD (n=3). **p<0.01, ***p<0.001 by the Unpaired t-test.

(E) LLC1 tumor cells were co-incubated with hCG (1 mg/ml, 0.026 mM; 13,000 IU/mg) and Prog (50 µM), or with beta-hCG (0.026 mM) and Prog for 24 h. Veh (hCG / beta-hCG): PBS; Veh (Prog + hCG / beta-hCG): ethanol + PBS. Cell viability was assessed by MTT. Data is plotted as percentage viability over untreated cells. Values represent arithmetic mean ± SD (n=3). ***p<0.001 by the Unpaired t-test. ns: non-significant.

(F) Experimental setup identical to (E). Lysates were probed with an anti-caspase-3 antibody by Western blot. The vertical gap in between columns representing pro- and cleaved-caspase 3 denotes splitting of the same blot to efficiently capture pro- and cleaved fragments separately. Blots were exposed to the same X-ray film to ensure equal exposure to chemiluminescent signals (raw data provided). Gapdh for a representative experiment is shown. 24 h data is represented.

Figure 5

Progesterone supplementation dampens the enhanced beta-hCG-mediated tumor growth observed in the absence of ovaries in beta-hCG transgenic mice

(A) Tumor volumes in transgenic (TG) mice, in ovariectomized transgenic vehicle treated (OVX-TG-Veh) mice, and in ovariectomized transgenic progesterone treated (OVX-TG-Prog) mice post-implantation of LLC1 tumor cells. Values represent arithmetic mean ± SD (n=7). **p<0.01, OVX-TG-Prog vs OVX-TG-Veh by Two-way ANOVA followed by the Bonferroni Multiple Comparison Test.

(B) Representative pictures of tumors in mice from the three groups on Day 30.

(C) RNA-seq analysis. Venn diagram indicating differentially-expressed genes in tumors excised from the different groups of mice. For OVX-TG-Veh, “LOW” and “HIGH” refer to comparisons with tumors from TG mice. For OVX-TG-Prog, “LOW” and “HIGH” refer to comparisons with tumors from OVX-TG-Veh mice (Refer Fig S8). The * indicates genes potentially influenced by Prog, where ovariectomy-induced changes are reversed upon Prog administration. For each group two tumors from two different mice belonging to the same group were included for RNA-seq analysis.

(D) Heat map depicting “pro-tumorigenic genes” (up-modulated upon ovariectomy and down-modulated upon progesterone administration) and “anti-tumorigenic genes” (down-modulated upon ovariectomy and up-modulated upon progesterone administration). Mouse figurines at the bottom of the figure represent LLC1 tumor volumes in the three groups of mice.

(E) Validation of genes represented in the heat map by qPCR. Ct values of each gene was normalized to actin and ΔΔCt method was applied for quantification of relative mRNA levels. **Values represent arithmetic mean fold change ± SD (n=3). *p<0.05, **p<0.01, ***p<0.001; OVX-TG-Veh vs TG by the Unpaired t-test.**

(F) Validation of genes represented in the heat map by qPCR. Ct values of each gene was normalized to actin and ΔΔCt method was applied for quantification of relative mRNA levels. Values represent arithmetic mean fold change ± SD (n=3). **p<0.01, ***p<0.001; OVX-TG-Prog vs OVX-TG-Veh by the Unpaired t-test.

(G) Immunohistochemical analysis depicting reactivity of antibodies against the indicated molecules in tumor sections derived from TG mice, OVX-TG-Veh mice or OVX-TG-Prog mice. Scale: 40 μm.

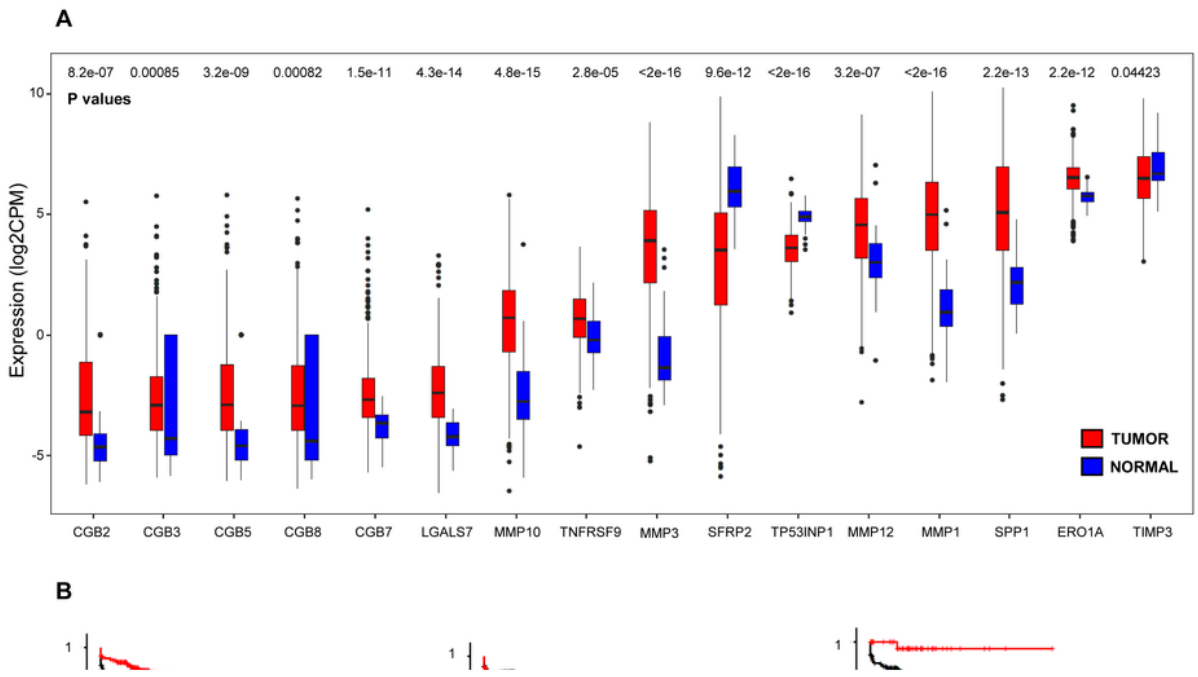

Figure 6

Progesterone-influenced molecular profile identified by RNA-seq in murine tumors displays clinical relevance

(A) Expression of the indicated genes in COAD (n=480) and normal tissue (n=41). The Wilcoxon test was employed to determine significance, depicted above respective bars.

(B) Survival analysis of COAD patients with either high expression or low expression of CLU (n, high/low=393/62), TP53INP1 (n, high/low=150/305), FOS (n, high/low=393/62), HSPA1B (n, high/low=380/75) or HSPA1A (n, high/low=382/73). The Logrank test was employed to determine significance, depicted in each panel.

Figure 7

Progesterone-influenced molecular profile identified by RNA-seq in murine tumors underscore the onco-protective nature of the pre-menopausal reproductive stratum in women

(A) Survival analysis of post-menopausal women (POST) with either high expression and low expression of MMP10 (in COAD; n, high/low=96/67), MMP3 (in GBM; n, high/low=4/39) or CGB3 (in LUAD; n, high/low=103/129). The Logrank test was employed to determine significance, depicted in each panel.

(B) Survival analysis of pre-menopausal women (PRE) with either high expression and low expression of MMP10 (in COAD; n, high/low=24/28), MMP3 (in GBM; n, high/low=0/16) or CGB3 (in LUAD; n, high/low=19/34). The Logrank test was employed to determine significance, depicted in each panel.

(C) Survival analysis of post-menopausal (POST) and pre-menopausal (PRE) women with high expression of LGALS7 (in COAD; n, post-menopause/pre-menopause=62/21), MMP1 (in GBM; n, post-menopause/pre-menopause=18/4), SPP1 (in GBM; n, post-menopause/pre-menopause=37/10) or CXCL9 (in GBM; n, post-menopause/pre-menopause=36/13). The Logrank test was employed to determine significance, depicted in each panel.

Figure 8

Graphical abstract summarizing the main findings of this study and their implication

Supplementary Files

This is a list of supplementary files associated with this preprint. Click to download.

- AGAROSEGELSrawdataSarkaretal.pdf
- BLOTSrawdataSarkaretal.pdf
- Supplementaryinformationadditionalmaterials.pdf